ACS Catalysis

RESEARCH ARTICLE

pubs.acs.org/acscatalysis

Aerobic Baeyer–Villiger Oxidation of Cyclic Ketones over Metalloporphyrins Bridged Periodic Mesoporous Organosilica

Eun-Young Jeong, Mohd Bismillah Ansari, and Sang-Eon Park*

Laboratory of Nano-Green Catalysis and Nano Center for Fine Chemical Fusion Technology, Department of Chemistry, Inha University, Incheon 402-751, Korea

Supporting Information

ABSTRACT: Highly ordered Metal-tetrakis(carboxyphenyl)porphyrin (Metal = Fe, Cu, Sn) bridged periodic mesoporous organosilicas (M-TCPP-PMO) with high surface area were synthesized from corresponding M-tetrakis(carboxyphenyl)porphyrin-silsesquioxanes as tetra-silanes by the sol–gel method. The Baeyer–Villiger oxidation of ketones to the corresponding esters using molecular oxygen as an oxidant over M-TCPP-PMOs was investigated. Fe-TCPP-PMO was found to exhibit higher catalytic activity than Cu-TCPP-PMO and Sn-TCPP-PMO. The high catalytic activity is attributed to the high-valent Fe-porphyrin on the wall of mesoporous silica along with cyclohexanone, which results in successful completion of the oxygen transfer step and generation of ε-caprolactone. The obtained results demonstrate that Fe-TCPP-PMO is a promising and efficient catalyst for the Baeyer–Villiger oxidation of ketones to esters using O_2 as the oxidant.

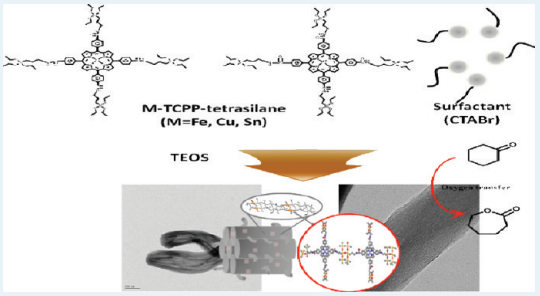

KEYWORDS: metalloporphyrin, periodic mesoporous organosilicas, high-valent Fe-porphyrin, aerobic Baeyer–Villiger oxidation

1. INTRODUCTION

Metalloporphyrins have attracted considerable interest because of their various physicochemical properties and their wide range of applications such as nonlinear optical materials,[1] engineered molecular building blocks,[2] bio- and optical sensors[3] and solar energy storage devices,[4] photodynamic therapy,[5] and metal adsorption.[6] Metalloporphyrins have been also studied in these systems as biomimetic catalysts[7] of enzymes such as the monooxygenases. A well-known monooxygenase, Fe porphyrin-based cytochrome P450, is nowadays evoking great interest because of its ability to catalyze a variety of oxidation reactions mimicking P450, such as alkene epoxidation and alkane hydroxylation with molecular oxygen.[8] However, the use of metalloporphyrin as a catalyst in homogeneous oxidation processes has several disadvantages.[9] For example, metalloporphyrin catalyzes reactions such as hydroxylation and epoxidation homogeneously, but the resulting homogeneous catalytic systems have the following drawbacks: (1) they do show low selectivity and (2) it is difficult to isolate metalloporphyrin from the product, which makes homogeneous catalysis an expensive procedure in commercial processes. Also, deactivation of active sites is caused by aggregation of porphyrin rings by $\pi-\pi$ interaction as the reaction proceeds.[10]

The above-mentioned problems could be solved by synthesizing metalloporphyrin-functionalized materials by the immobilization onto supports such as alumina,[11] bentonites,[12] montmorillonites,[13] and layered double hydroxide,[14,15] and silica,[3,16] which could also be used as heterogeneous catalysts.

Although many research groups have attempted to functionalize metalloporphyrin in mesoporous silica, these systems are prone, however, to common leaching problems and limited accessibility to the reactants. Further, catalyst stability is necessary for the reuse and recovery of metalloporphyrin. These key issues can be resolved by attaching organic functions to the siliceous wall by using organic-bridged alkoxysilane precursors entirely or partially with a silica source; this assembly is termed periodic mesoporous organosilica (PMO).

PMO, synthesized from an organosilane precursor, is a special type of ordered mesoporous silica in which organic moieties are integrated into the silica framework entirely or randomly to form hybrid organic–inorganic materials. In particular, PMOs are well suited for use as catalysts because of the advantages they offer, such as easy accessibility, rapid diffusion, and favorable mass transfer for substrates into and out of the mesopores.[17−21] Several reviews have been published describing the developments in the fields of catalysis applications of periodic mesoporous silica. Arai et al. investigated the catalytic activity of chromium-containing periodic mesoporous organosilicas in the aerial oxidation of cyclohexane and ethylbenzene.[22] Li et al. demonstrated aluminum-containing mesoporous ethane-silicas as efficient catalysts for the alkylation of 2,4-di-*tert*-butylphenol by cinnamyl alcohol to yield a flavan.[23] Li et al. reported a Pd/Ph-

Received: January 31, 2011
Revised: May 4, 2011
Published: June 01, 2011

PMO catalyst which shows high catalytic activity in the water mediated Ullmann coupling reaction.[24]

Short aliphatic chain-like methane, ethane, and ethylene, as well as aromatic groups of phenylene,[20] biphenylene,[25] and xylene have been also used as bridging organic moieties, mostly in the form of disilanes. However, organosilane precursors in the form of trisilanes and tetrasilanes have rarely been used.[26] Jaroniec and Grudzien synthesized an ethane-isocyanurate-bridged PMO simply by using tris[3-(trimethoxysilyl)propyl]isocyanurate and 1,2-bis(triethoxysilyl)ethane in the presence of a triblock copolymer.[27] Further, Ozin et al. synthesized C60−PMO by assembling C60 and tetraethyl orthosilicate (TEOS) with P123.[28] We recently reported the synthesis of porphyrin-bridged PMOs with high reproducibility by co-condensation using tetrakis-(carboxyphenyl)porphyrin (TCPP)-silsesquioxane and sodium metasilicate in the presence of P123 (EO20PO70EO20) at a highly acidic concentration.[29]

M-tetrakis (carboxyphenyl)porphyrins (M = Fe, Cu, Sn) as an organic moiety are integrated inside the PMO channel walls with a maximum loading of 20%; then, bridge-bonded M-TCPP (M = Fe, Cu, Sn) inside the channel walls does not block the mesopores. In addition, the M-TCPP-PMO system can be employed in bio- and physicochemical processes owing to some interesting properties of metalloporphyrin,[30−34] such as its electron transfer function, luminescence property, and can also perform oxidation as a model of cytochrome P450 monooxygenases.[35]

Baeyer−Villiger oxidation of ketones has received considerable attention in organic synthesis because products such as lactones or esters are very important intermediates in the chemical and drug industry.[36,37] One of the reported methods for converting ketones into esters is the Baeyer−Villiger oxidation with Fe_2O_3 as Lewis-acid metal using molecular oxygen[38] because Lewis-acid metals can catalyze the peroxy species attacking the carbonyl group. In the case of Fe-porphyrin, the high-valent oxo-Fe-porphyrin species, which combines cyclohexanone to generate ε-caprolactone during the oxygen transfer step. Therefore, the use of Fe-TCPP as catalysts has previously proved to be favorable for the generation of an effective oxidizing agent for Baeyer−Villiger oxidation when oxygen was combined with an aldehyde, presumably with the intermediate appearance of acyl radicals and peracids. Further, oxidants such as peracids, *m*-chloroperbenzoic acid (*m*-CPBA), and bis(trimethylsilyl)-peroxide, which are commonly used to carry out Baeyer−Villiger oxidation, potentially generate harmful wastes. Therefore, many efforts have been made to develop catalytic oxidation methods that employ molecular oxygen, which is an environmentally friendly (i.e., green) oxidant. The molecular oxygen has significant advantages because of safe, cheap, faster kinetics, higher yield, higher active oxygen content, and better reproducibility. Despite these facts, there are only a few reports on the use of molecular oxygen for Baeyer−Villiger oxidation. Here, we report the use of molecular oxygen for the Baeyer−Villiger oxidation catalyzed by metalloporphyrin bridged periodic mesoporous silica in a shorter time and lower temperature. This is notable as it is the first report in the field of periodic mesoporous organosilica.

In this study, we focused on the synthesis of PMOs with M-TCPP-silsesquioxanes (M = Fe, Cu, and Sn) as tetrasilanes. M-TCPP-PMOs described herein were synthesized by direct co-condensation using a thermal sol−gel method. M-TCPP-tetrasilanes linked in the PMO (hereafter referred to as M-TCPP-PMO) were synthesized by the self-assembly of M-TCPP-tetrasilanes together with TEOS as a surplus silica source and cetyltrimethylammonium bromide (CTABr) (Scheme 1). The synthesized M-TCPP-PMOs were used to catalyze the Baeyer−Villiger oxidation with molecular oxygen as the oxidant.

Scheme 1. Synthesis Route of M-Tetrakis(4-carboxyphenyl)porphyrin-Periodic Mesoporous Organosilicas

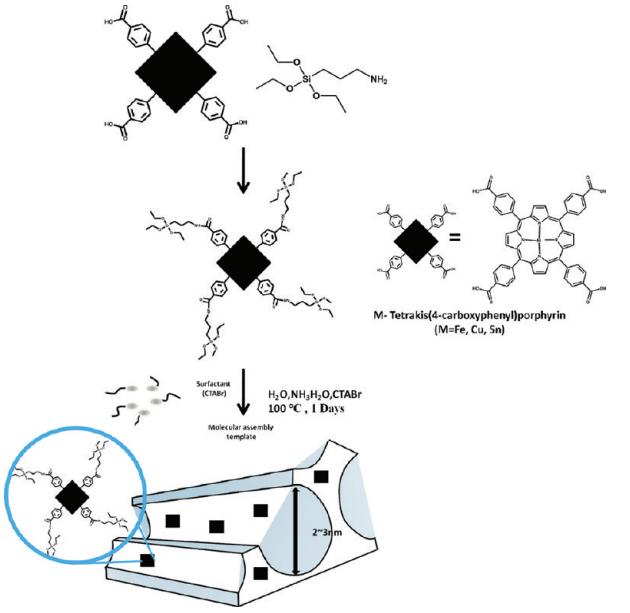

2. EXPERIMENTAL SECTION

2.1. Reagents and Materials. All chemicals for synthesizing materials and testing catalytic activity were also purchased from Sigma-Aldrich Corporation, St. Louis, MO (U.S.A.) and directly used without further purifications.

2.2. Characterization. The X-ray diffraction (XRD) patterns were obtained by using a Rigaku Multiflex diffractometer with a monochromated high-intensity Cu Kα radiation (λ = 1.54 Å). Scanning was performed under ambient conditions over the 2θ range of 0.7−5° at the rate of 0.1°/min (20 kV, 10 mA). The scanning electron microscope (SEM) images were observed using a JEOL 630-F microscope. Before the measurement, the samples were dispersed onto a steel plate surface and coated with Pt metal. Transmission electron microscope (TEM) images were observed using a JEM-3011 instrument (JEOL) equipped with a slow-scan CCD camera operating at 300 keV. Solid-state NMR spectra were collected through a DSX Bruker NMR 600 MHz. The N_2 adsorption−desorption isotherms and pore characterization were obtained by using a Micromeritics tristar apparatus at liquid N_2 temperature. Pore diameter was calculated by using the Barrett−Joyner−Halenda (BJH) method from the adsorption branches. The tetrakis(4-carboxyphenyl)porphyrin was analyzed by UV−vis-NIR spectroscopy (Solidspec-3700). Fe-TCPP-PMO was checked by electron paramagnetic resonance (EPR) equipment. (JEOL FA200 instrument). Matrix-assisted laser desorption/ionization-time of flight (MALDI-TOF) analysis was used to confirm the purity of the final products. Metal concentration was measured using Inductively Coupled Plasma Spectrometer (Optima 7300DV).

2.3. Synthesis of Tetrakis(4-carboxyphenyl)porphyrin (TCPP)[29]. Pyrrole (2.33 mmol) and 4-carboxybenzaldehyde

dx.doi.org/10.1021/cs200163r |*ACS Catal.* 2011, 1, 855–863

Table 1. Physicochemical Properties for M-TCPP-PMO-*n* (M = Fe, Cu, Sn ; *n* = 10%, 20%)

		N_2 adsorption−desorption analysis			XRD			UV−vis spectroscopy
sample	TEOS:M-TCPP-tetrasilane[a]	surface area ($m^2\ g^{-1}$) [b]	pore diameter (nm) [c]	total pore volume ($cm^3\ g^{-1}$) [d]	d_{100}[e] (nm)	a_0[f] (nm)	wall thickness (nm) [g]	Soret band (nm)
Fe-TCPP-PMO-10%	90:10	871	2.07	0.80	3.8	4.42	2.35	409
Fe-TCPP-PMO-20%	80:20	530	1.94	0.71	4.03	4.69	2.75	410
Cu-TCPP-PMO-10%	90:10	1087	2.47	0.91	4.01	4.62	2.20	416
Cu-TCPP-PMO-20%	80:20	859	1.97	0.60	4.06	4.72	2.76	417
Sn-TCPP-PMO-10	90:10	450	1.67	0.34	4.3	5.00	3.33	420
Sn-TCPP-PMO-20	80:20	350	1.62	0.28	4.6	5.35	3.71	419

[a] M-TCPP-tetrasilane precusor into the gel during the synthesis step on a weight ratio. [b] Surface area calculated by the BET method. [c] Pore size diameter calculated by BJH method. [d] Total pore volume recorded at $P/P_0 = 0.995$. [e] Inter planar spacing. [f] a_0 (nm)= $2d_{100}/\sqrt{3}$. [g] Wall thickness = a_0 − pore size.

(2.33 mmol) were dissolved in 100 mL of propionic acid. The mixture was refluxed for 4 h, and then this crude product was cooled to room temperature. After cooling to room temperature, the mixture was added to 100 mL of methanol and chilled in an ice bath with stirring. The deep-purple crystals were filtered and washed with methanol and hot water. The resulting solid was dissolved in chloroform with 2% acetone and purified by column chromatography over silica gel using chloroform as eluent. UV−vis data for TCPP in THF. λmax (nm): 416, 513, 547, 591, 647 nm. The C/N ratio of TCPP was obtained by elemental analysis (C/N).[29] Maldi-TOF spectrum: 791 [M+H]+.

2.4. Synthesis of Cu-Tetrakis(4-carboxyphenyl)porphyrin (Cu-TCPP). The TCPP (260 mg) was dissolved in 70 mL of dimethylformamide (DMF). Then 1.82 mmol of $CuCl_2 \cdot 2H_2O$ was added. The mixture was refluxed at 80 °C during 1 h and cooled at room temperature. Acetone was added to precipitate the Cu-TCPP. The Cu-TCPP were washed with acetone and dried. UV−vis data for Cu-TCPP in THF. λmax (nm) 417, 540, 583 nm.

2.5. Synthesis of Sn-Tetrakis(4-carboxyphenyl)porphyrin (Sn-TCPP). The TCPP (1.63 mmol) and anhydrous tin dichloride (4.9 mmol) were dissolved in 200 mL of tetrahydrofuran (THF). The pyridine in small portions was added and then the reaction mixture was refluxed for 6 h with stirring. After completion of the reaction, the solution was filtered out. The crude product was dissolved in toluene and chromatographed over an alumina column previously. UV−vis data for Sn-TCPP in THF. λmax (nm) 421, 519, 553, 595, 650 nm.

2.6. Synthesis of Fe-Tetrakis(4-carboxyphenyl)porphyrin (Fe-TCPP). The TCPP (0.081 mmol) was dissolved in 30 mL of argon-purged dimethylformamide (DMF). Then 0.6 mmol of iron chloride tetrahydrate was added. The mixture was refluxed at 120 °C for 4 h and cooled at room temperature under nitrogen gas for 4 h, after that in an atmosphere of air for 2 h. The solvent was removed and washed with small portions of deionized water to remove the excess of metal(III) salt and was purified by chromatography in a silica column in DMF. UV−vis data for Fe-TCPP in DMF. λmax (nm) 420, 504, 560, 684 nm.

2.7. Synthesis of M-TCPP-Silsesquioxane (M = Fe, Cu, and Sn). In a round-bottom flask, 3-aminopropyltriethoxysilane (4 mmol) and dicyclohexyl carbodiimide (4 mmol) were suspended in 50 mL of tetrahydrofuran (THF). The M-TCPP (1 mmol) was dissolved in 5 mL of THF and added drop-wise. The flask was evacuated and flushed with nitrogen gas. The mixture was refluxed for overnight under nitrogen atmosphere. After cooling down to room temperature, the product was washed with petroleum ether. ^{13}C CP MAS NMR spectrum: δ 13 (CH_2-$\underline{C}H_2$-Si), 25 (CH_2-$\underline{C}H_2$-CH_2), 45 (NH-$\underline{C}H_2$-CH_2), 116 and 135 (β-pyrrolic carbon), 143 (α-pyrrolic carbon), 165.9 (Phenyl-$\underline{C}$O-NH).

2.8. Synthesis of M-TCPP-periodic mesoporous silica (M = Fe, Cu, and Sn). CTABr (0.36 mmol) was dissolved in 16 wt % $NH_3 \cdot H_2O$ (54.8 mmol), and the solution was stirred at 50 °C for 1 h. After cooling to room temperature, TEOS were added to the solution and stirred until a homogeneous solution was obtained. To this solution, M-tetrakis(carboxyphenyl)porphyrin-silsesquioxane was added, and the resulted mixture was stirred at 50 °C for 10 h, followed by aging at 100 °C for 1 day. The mixture was then cooled to room temperature, the resultant solid was filtered and air-dried overnight. The solid product was filtered and washed with copious amount of water and ethanol. And further removal of the surfactant was performed by Soxhlet extraction using ethanol and hydrochloric acid (v:v = 97:3) for 4 h. To obtain M-TCPP-PMOs with varying amount of M-TCPP-tetrasilane contents, different weight ratios of M-TCPP-tetrasilane and TEOS were used in the procedure as summarized in Table 1. The C/N ratio of M-TCPP-PMO was obtained by elemental analysis (C/N). Fe-TCPP-PMO-20 = Calcd: 6.42, Anal: 6.25 ; Cu-TCPP-PMO-20 = Calcd: 6.42, Anal: 6.30 ; Sn-TCPP-PMO-20 = Calcd: 6.42, Anal: 6.45.

2.9. Catalytic Test. Baeyer−Villiger oxidation of ketones (cyclopentanone, cyclohexanone, cycloheptanone, cyclooctanone, 2-adamantanone, 2-methylcylohexanone, 4-methylcyclohexanone) was conducted in the liquid-phase with molecular oxygen. In a typical reaction procedure, 25 mg of catalyst (preactivated at 438 K prior to use) was mixed with 15 mL of 1,2-dichloroethane. To this mixture, 0.1 mmol of substrate and benzaldehyde (0.3 mmol) were added and heated at 313 K with molecular oxygen. The reaction mixture was withdrawn and subjected to GC analysis (Young lin 6100, HP-INNOWAX capillary column, FID detector).

Catalyst leaching was studied at 313 K under similar conditions of oxidation (catalyst = 25 mg, temp. = 313 K and time = 5 h). After the 5 h reaction, the catalyst was separated by filtration. In the case of the recyclability test, after washing with 1,2-dichloroethane and drying, the catalyst was used for a subsequent cycle for Baeyer−Villiger oxidation.

3. RESULTS AND DISCUSSION

3.1. Characterization of M-TCPP-PMO (M = Fe, Cu, Sn). The synthesis of M-TCPP-PMOs from TEOS and M-TCPP-tetrasilanes were described in Scheme 1. The synthetic conditions, the pore sizes, cell unit parameters, and the pore volume of these

dx.doi.org/10.1021/cs200163r |ACS Catal. 2011, 1, 855–863

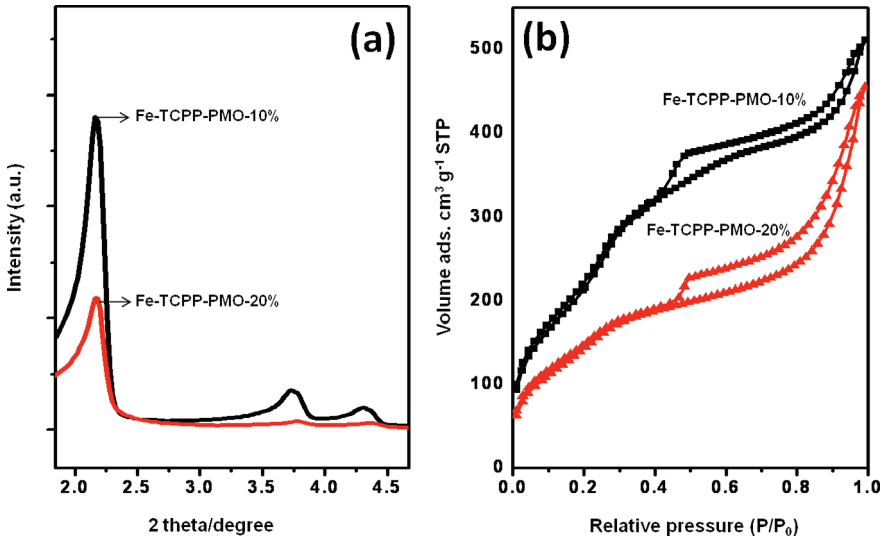

Figure 1. XRD patterns (a) and nitrogen adsorption−desorption isotherms (b) of samples Fe-TCPP-PMO-10% and Fe-TCPP-PMO-20%.

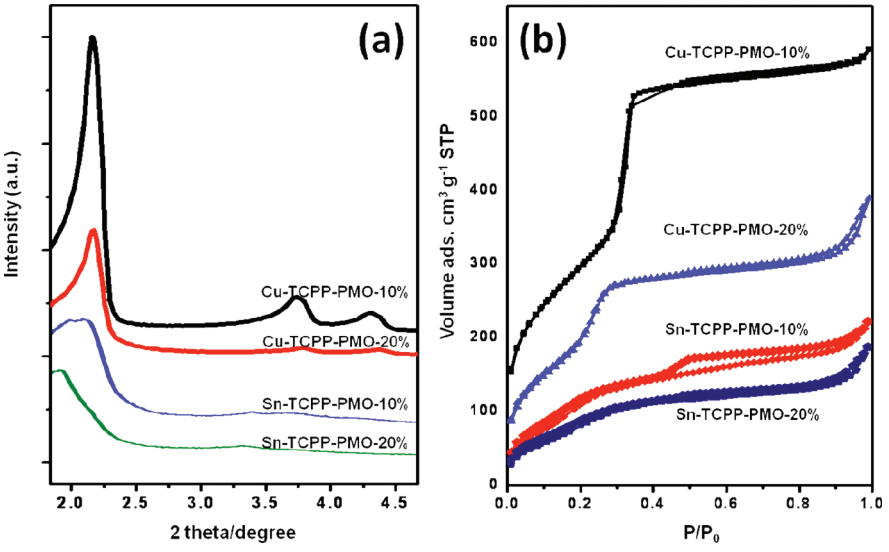

Figure 2. XRD patterns (a) and nitrogen adsorption−desorption isotherms (b) of Cu-TCPP-PMO-10%, Cu-TCPP-PMO-20% and Sn-TCPP-PMO-10%, Sn-TCPP-PMO-20%.

mesoporous materials are summarized in Table 1. The ordered M-TCPP-PMO-*n* (*n* = 10%, 20%) with high surface area were synthesized at base condition (54.8 mmol of 16 wt % $NH_3 \cdot H_2O$) via the self-assembly of M-TCPP-tetrasilanes (as reported by us earlier) together with TEOS as a surplus silica source and cetyltrimethylammonium bromide (CTABr) at 100 °C for 24 h.

Figure 1a shows the low angle XRD powder patterns of Fe-TCPP-PMO-10% and Fe-TCPP-PMO-20%, prepared via the CTABr templating thermal method. All XRD patterns of CTABr-templated Fe-TCPP-PMOs exhibited at least three well-resolved diffraction peaks at 2θ of 2−2.5 and two peaks at higher degree in the range of 2θ of 3.5−4.5 (Figure 1a).

An intense peak at the (100) diffraction is observed on both samples and in good agreement with reported patterns from MCM-41 material.[39] The XRD patterns indicate that the intensity of the d_{100} reflection decreases as the Fe-TCPP- silsesquioxane precursors: TEOS ratio increases in the reaction mixtures.

The low-angle powder XRD patterns of Cu-TCPP-PMO-*n* and Sn-TCPP-PMO-*n* are shown in Figure 2a. Cu-TCPP-PMO-*n* showed one well-resolved diffraction peaks corresponding to the mesostructure of the hexagonal space group symmetry *P6mm*. Weak peaks were observed at 2θ = 2−5° for Sn-TCPP-PMO-*n*, suggesting worse mesostructural features with loading of Sn-TCPP.

Nitrogen adsorption−desorption isotherms for Fe-TCPP-PMO-*n* materials were found to be type IV curves, with a capillary condensation step, characteristic of mesoporous materials (Figure 1b). When the Fe-TCPP tetra silane content increases from 10% to 20%, Nitrogen adsorption−desorption isotherms of the Fe-TCPP-PMO-*n* materials exhibited a tendency to change isotherms. The position of the capillary condensation branch shifts toward lower relative pressure which indicates smaller pore sizes with increasing Fe-TCPP tetra silane contents. The Fe-TCPP-PMO-*n* samples exhibit size distributions of pores with maxima shifting from about 2.07 to 1.94 nm as the % Fe-TCPP tetra silane in the synthesis gel increases from 10% to 20%.

dx.doi.org/10.1021/cs200163r |*ACS Catal.* 2011, 1, 855–863

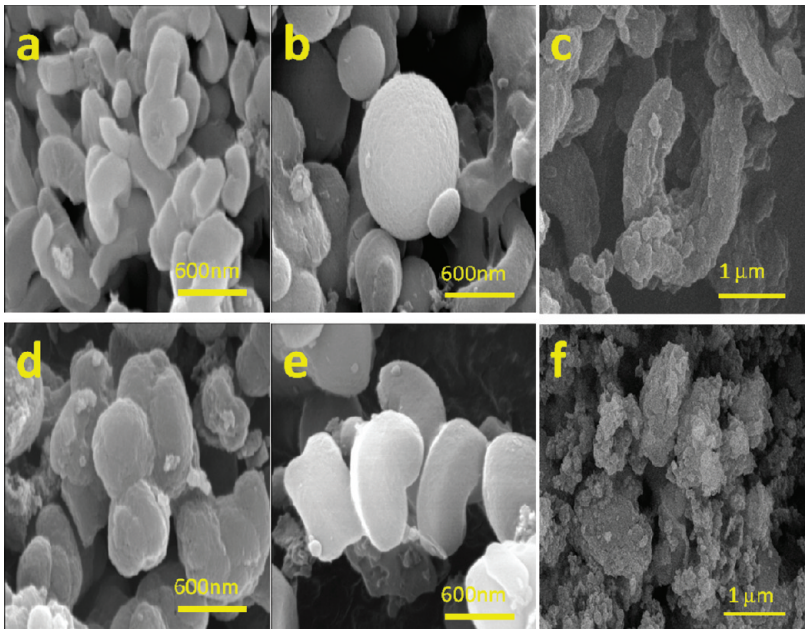

Figure 3. SEM images of samples Fe-TCPP-PMO-10% (a), Cu-TCPP-PMO-10% (b), Sn-TCPP-PMO-10% (c), Fe-TCPP-PMO-20% (d), and Cu-TCPP-PMO-20% (e), Sn-TCPP-PMO-20% (f).

Nitrogen adsorption−desorption isotherms for Cu-TCPP-PMO-*n* show type-IV isotherms, with a sharp increase in adsorption at $P/P_0 = 0.25-0.38$, indicating that this material had uniform mesopores (Figure 2b). The BJH (Barrett−Joyner−Halenda) pore diameter and BET (Brunanuer−Emmett−Teller) surface area of the Cu-TCPP-PMO-10% and Cu-TCPP-PMO-20% samples were 2.47 nm, 1087 $m^2\ g^{-1}$, and 1.97 nm, 859 $m^2\ g^{-1}$, respectively. All the Nitrogen adsorption−desorption isotherms of the Sn-TCPP-PMO-*n* were type IV isotherms (Figure 2b). The pore diameters given from BJH distribution curves for the Sn-TCPP-PMO-*n* samples decreased, as the amount of Sn-TCPP tetra silane in the synthesis gel increased. In contrast, the wall thickness increased.

The trend of mesopore shrinkage with increasing M-TCPP tetra silanes loading is also exhibited by changes in the surface area and total pore volume, which indicate that the mesostructural feature gets worse with higher loading of M-TCPP tetra silanes groups. Specific surface areas and mesopore diameters for different M-TCPP-PMO-*n* are shown in Table 1. Also, each of these three materials displays a narrow pore size distribution (Supporting Information, Figures S1, S2, and S3).

Another more interesting finding was subsequent morphological control when the different amounts of M-TCPP-silsesquioxanes were used. SEM images of Fe-TCPP-PMO-10% and Fe-TCPP-PMO-20% were shown as Figure 3a,d. The SEM images clearly show the difference of morphology. In these cases, the unique morphology of the catalyst can be observed by direct functionalization of Fe-TCPP tetra silane in the silica wall. Instead of fibrous type, bean (Fe-TCPP-PMO-10%) morphology was obtained, but Fe-TCPP-PMO-20% could be obtained with irregular dumbell type morphology. SEM images of Cu-TCPP-PMO-*n* and Sn-TCPP-PMO-*n* were also shown as Figure 3b,c,e,f. Sphere (Cu-TCPP-PMO-10%) and bean (Cu-TCPP-PMO-20%) morphologies were obtained, but Sn-TCPP-PMO-*n* could be obtained with irregular bar type morphology. TEM images of M-TCPP-PMO-*n* are consistent with the powder XRD results,

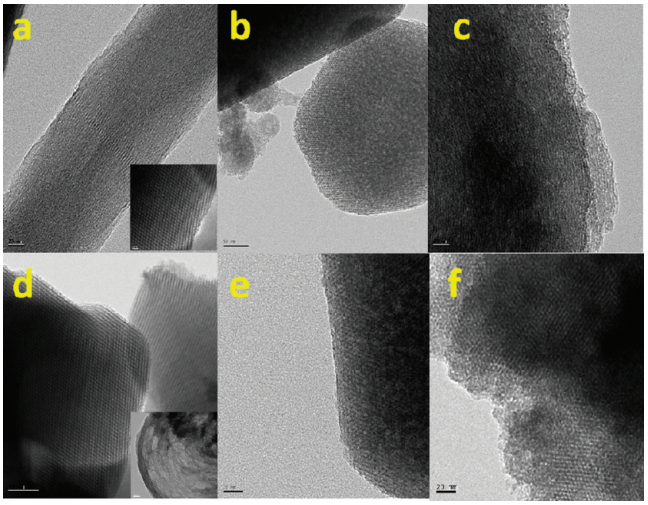

Figure 4. TEM images of samples Fe-TCPP-PMO-10% (a), Cu-TCPP-PMO-10% (b), Sn-TCPP-PMO-10% (c), Fe-TCPP-PMO-20% (d) and Cu-TCPP-PMO-20% (e), Sn-TCPP-PMO-20% (f).

showing hexagonal symmetry mesopores throughout the samples (Figure 4).

The Fe-tetrakis(4-carboxyphenyl)porphyrin (Fe-TCPP) unit integrated into the mesoporous silica framework was checked by DR-UV spectroscopy (Figure 3A). The UV−vis spectra of the Fe-TCPP-PMO-*n* exhibited one Soret band in the spectral range of 409−411 nm accompanied by two Q bands, respectively in the 573 and 614 nm spectral ranges. The Soret band of Fe-TCPP at 409 nm reveals that Fe-TCPP on the wall of mesoporous silica wall has been prepared. This Soret band is characteristic of internal $\pi \rightarrow \pi^*$ transitions of the ligand Fe(III)-porphyrins. The Q bands of Fe-TCPP are shifted and partially overlapped, as previously reported in the literature for other metalloporphyrins of the same type. The Q bands of Fe-TCPP-PMO are typical of

dx.doi.org/10.1021/cs200163r |*ACS Catal.* 2011, 1, 855–863

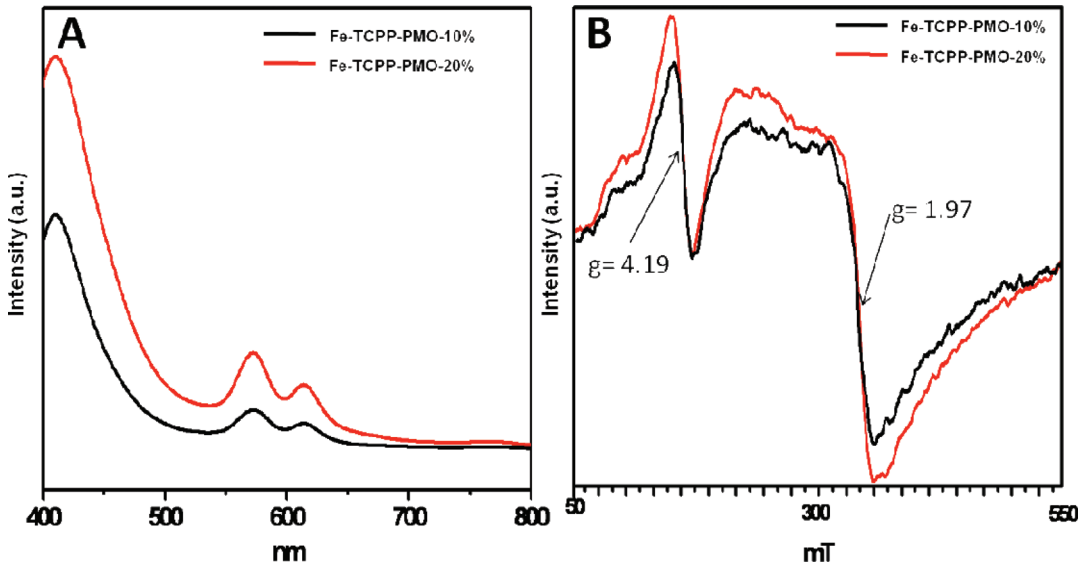

Figure 5. UV−vis spectra (A) and EPR spectra (B) of samples Fe-TCPP-PMO-10% and Fe-TCPP-PMO-20% (The Fe-TCPP-PMO-*n* samples were pretreated in an in situ cell at 150 °C under a vacuum system prior to subjecting to EPR spectra).

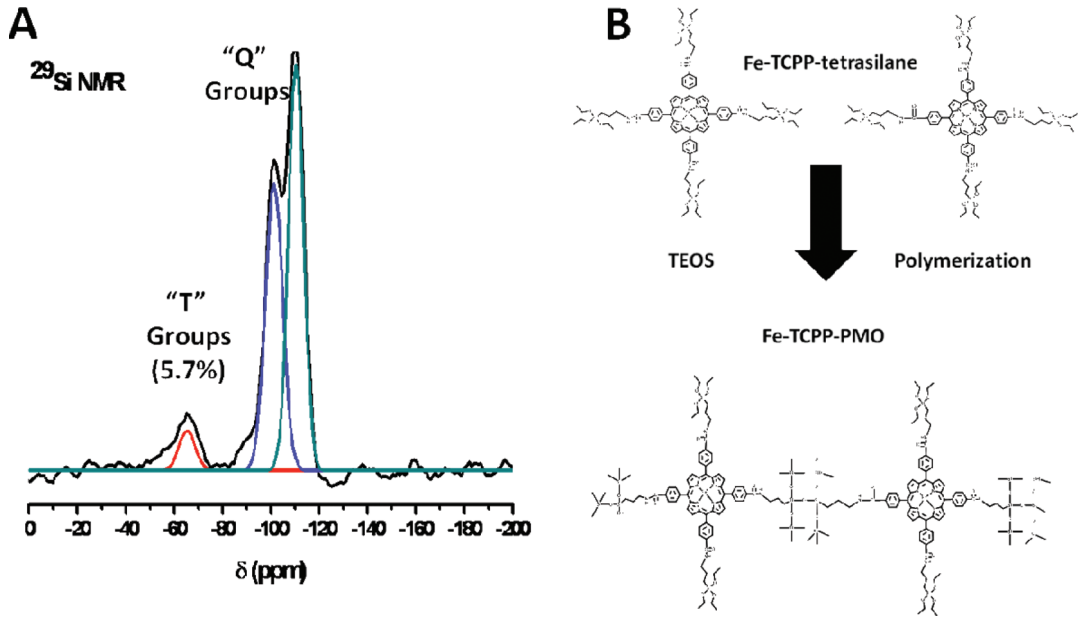

Figure 6. ^{29}Si CP MAS NMR spectrum (A) and chemical reaction path for the formation (B) of Fe-TCPP-PMO-20%.

those of high-spin Fe(III)-porphyrins. The Q bands between 573 and 614 nm are also attributed to d-d transitions of the iron(III). The peak of Soret band and Q-bands for different Cu-TCPP-PMO-*n* and Sn-TCPP-PMO-*n* are shown in Table 1 and experimental sections 2.4 and 2.5.

To confirm the presence of the Fe-TCPP tetra silane moieties inside the PMO material, ^{29}Si CP-MAS NMR spectroscopic measurements and EPR spectroscopy were carried out (see Figure 5B ; Figure 6A). The presence of Fe(III) species in Fe-TCPP-PMO-*n* could be easily checked by other technique of ESR spectroscopy. Fe-TCPP-PMO-10% and Fe-TCPP-PMO-20% exhibit a similar ESR spectrum with a high-spin Fe(III) signal at g = 1.97 (Figure 5B), and it was also observed representing the formation of the Fe-TCPP intra mesoporous wall. The signal at g = 4.2 is assigned to Fe(III) in a distorted framework tetrahedral coordination. Additionally, an increased content from Fe-TCPP tetra silane moieties is accompanied by a gradual increase of the ESR signal intensity in the magnetic field at g = 2.0006. Figure 6 exhibits the ^{29}Si NMR spectrum and chemical reaction path for the formation of the Fe-TCPP-PMO-20% after surfactant removal. The red, blue, and green line in Figure 6A represents Gaussian deconvolution peaks by integration of ^{29}Si NMR spectrum which is needed for calculation of Q and T groups. This spectrum shows two parts of major peaks, about 'T' group and 'Q' group, centered at the −65 ppm ('T' Group) and −87 ppm, −100 ppm, −110 ppm ('Q' Group). These two regions are related to the R-Si$(OSi)_3$ and Si$(OSi)_3(OH)$, Si$(OSi)_4$ species, respectively, where the R group is the tetrasilane organic group (Figure 6B). The Q^4/Q^3 ratio for Fe-TCPP-PMO-20% was found to be 1.44. T^2

dx.doi.org/10.1021/cs200163r |*ACS Catal.* 2011, 1, 855–863

Table 2. Catalytic Results of Baeyer-Villiger Oxidation of Cyclohexanone Using Molecular Oxygen by Various Catalysts

				yield over ε-caprolactone at different reaction times (%)[a]			
entry	catalyst	TOF[f]	metal contents (%)	0.5 h	1 h	3 h	5 h
1	MCM-41[b]		0	0	0	3.4	7.7
2	Fe-TCPP-PMO-10%	264	2.0	12.5	30.5	42.6	68
3	Fe-TCPP-PMO-20%	411	3.7	40.7	77.2	100	100
4	Fe-TCPP[c]	73		2.01	16.3	32.5	62
5	Cu-TCPP-PMO-20%[d]	103	3.2	3.2	11.1	16.6	23.7
6	Sn-TCPP-PMO-20%[e]	63	2.7	1.6	6.5	7.2	10.4

[a] Reaction conditions: 313 K, 5 h, Co-reductant; 3 mmol of benzaldehyde, catalyst 25 mg, substrate: 1 mmol. [b] Pure MCM-41. [c] Fe-TCPP complex (homogeneous). [d] Cu-TCPP-PMO-20% for a comparison of catalytic activity with Fe-TCPP-PMO. [e] Sn-TCPP-PMO-20% for a comparison of catalytic activity with Fe-TCPP-PMO. [f] Catalytic activity by metal porphyrin (Turnover number), minute $^{-1}$.

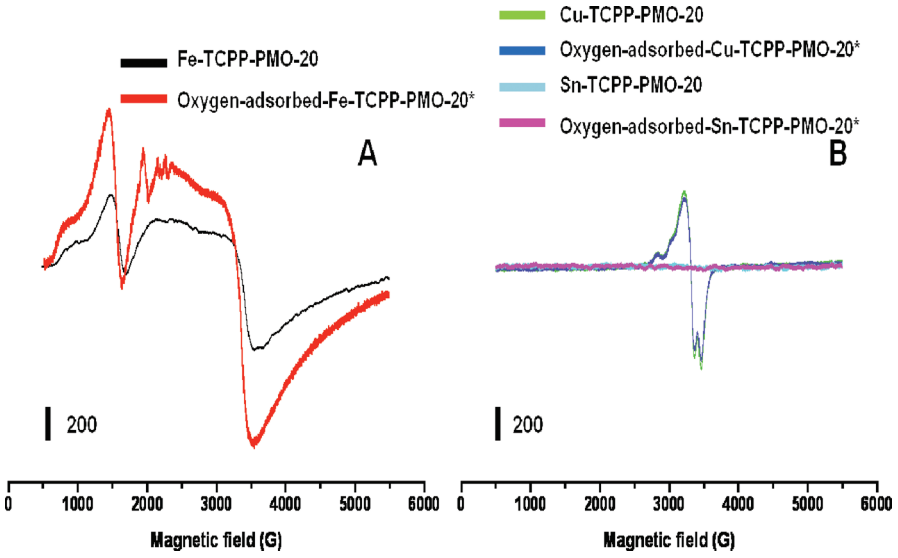

Figure 7. EPR spectra of M-TCPP-PMO-20% adsorption test using molecular oxygen ((A) Fe-TCPP-PMO-20% and (B) Cu, Sn-TCPP-PMO-20%, adsorption time; 360 min at 77 K).

[R-Si(OSi)$_2$(OH), d = −57.3]; T^3 [R-Si(OSi)$_3$, d = −65]; Q^2 [Si(OSi)$_2$(OH)$_2$, d = −87]; Q^3 [Si(OSi)$_3$(OH), d = −100.0]; Q^4 [Si(OSi)$_4$, d = −110.0].

3.2. Catalytic Activities of M-TCPP-PMO-*n* over Baeyer−Villiger Oxidation with Molecular Oxygen. Recently, Baeyer−Villiger oxidation with molecular oxygen can be performed by metalloporphyrin as a green approach. In this context, Fe-TCPP-PMO which has similar cytochrome P450 monooxygenase properties was first applied to the catalytic Baeyer−Villiger oxidation which is important to produce products such as lactones or esters that are very important intermediates in the chemical and drug industry. Cyclopentanone, cyclohexanone, cycloheptanone, cyclooctanone, adamantanone, 2-methylcyclohexanone, and 4-methylcyclohexanone were chosen as ketones with molecular oxygen as an oxidant. The catalytic results of Baeyer−Villiger oxidation of cyclohexanone using molecular oxygen and various catalysts are presented in Table 2. As Table 2 indicates, the best yield was obtained by using Fe-TCPP-PMO-20% in comparison to various other metal catalysts, with 100% yield over ε-caprolactone within 3 h.

The blank experiments with MCM-41 and different catalysts (Sn, Cu-TCPP-PMO, homogeneous Fe-TCPP) have less catalytic activity in comparison to Fe-TCPP-PMO-20%, showing that the catalytic activity is associated with the metal components and heterogeneous catalyst.

To estimate the effect of increasing Fe-TCPP in the siliceous wall, the Baeyer−Villiger oxidation was carried out with cyclohexanone as a substrate. The activities of Fe-TCPP-PMO-10% and -20% reached 68% and 100% of yield, respectively. Especially, the activity of Fe-TCPP-PMO-20% reached 100% during 3 h. There was significant increase of product. It was indicated that the catalytic activities are associated with Fe-TCPP center trapped within the mesoporous silica. Fe TCPP is able to activate molecular oxygen as an oxidant. The high-valent oxo-iron species combines cyclohexanone for generating ε-caprolactone during oxygen transfer step (Table 2; entry 1, 2, 3).

To check the role of the heterogeneous catalyst in comparison to the homogeneous catalyst in this liquid-phase reaction, homogeneous Fe-TCPP, FeTCPP-PMO-10%, and Fe-TCPP-PMO-20% catalysts were tested, and the results are also presented in Table 2. The Fe-TCPP-PMO-10 and -20% catalysts as heterogeneous catalysts gave a higher yield of ε-caprolactone than the reaction result using homogeneous catalysts; it was due to the short channels providing easy access and rapid diffusion and favorable mass transfer. The mesoporous structure, mesopore channel orientations offer the overall diffusion and mass transfer of substrates.

dx.doi.org/10.1021/cs200163r |ACS Catal. 2011, 1, 855–863

The possible presence of iron-oxo porphyrin was confirmed by EPR spectra, as show in Figure 7. Also Sn-TCPP-PMO and Cu-TCPP-PMO were checked by EPR spectroscopy. The EPR method was applied to the investigation of adsorption of oxygen on the M-TCPP-PMO. In the case of oxygen adsorbed Fe-TCPP-PMO-20%, a derivative radical-like feature has been found with a signal at $g = 2.0049$ and accompanied by a broad signal at $g = 3.35$. As shown in this result, this signal can be attributed to the oxygen species adsorbed on Fe-TCPP in the siliceous wall which can be assigned to a oxo-Fe(IV) porphyrin π-cation radical [Fe^{IV}=O $Por^{+\cdot}$] where Por = poryphyrin. Also, J/D is the ratio of exchange coupling to the zero-field splitting parameter of [Fe^{IV}=O]$^{2+}$. The ratio $J/D = 0.31$ is close to the Fe-Por model studied by Fujii et al (Table 3).[40] Other materials could not change the spectrum during the oxygen adsorption test.

The Baeyer–Villiger oxidation of various cyclic ketones catalyzed by the Fe-TCPP-PMO-20% was examined under atmospheric dioxygen (Figure 8). Among the cyclic ketones, the six-membered cyclic ketone was more efficiently oxidized than cyclopentanone under the same reaction conditions. This reaction behavior could be explained by substrates with steric configuration favoring the conversion owing to the existence of the large ring of the metalloporphyrin catalyst.

We further explored the use of other cyclic ketones, namely, seven-membered cyclic ketones and eight-membered cyclic ketones, for the Baeyer–Villiger reaction under similar reaction conditions. Unfortunately, the decrease in product yield (85 and 82%, respectively) was observed even increasing bulkiness of the substituent. Here, both Fe-TCPP-PMO-20% catalysts gave perfect selectivity toward only one desired product. In addition, the catalysts also had high durability which was demonstrated by a recyclability test as shown in Figure 8. The reused catalyst also exhibited good catalytic activity up to four catalytic runs with small loss in yield.

Figure 9 shows that the increasing rate of conversion over Fe-TCPP-PMO-20% was higher than those over Fe-TCPP-PMO-10%. These results could be explained by higher loading of active sites on Fe-TCPP-PMO-20%. It is well indicated that the high-valent Fe-TCPP π-cation radicals as active sites have great influence on liquid-phase heterogeneous catalytic reactions. Moreover, the substituent on the six-membered cyclic ketones was also investigated. The steric effects of reactants could be

Table 3. ESR Parameters of Oxoiron(IV) Porphyrin π-Cation Radical Complexes of Oxygen Adsorbed Fe-TCPP-PMO-20%[a]

entry	g_y	g_x	g_z	J/D
A (~0 min)	4.19		1.97	
B (~30 min)	4.20		1.97	
C (~360 min)	4.19	3.3	1.97	0.29
D (1 day)	4.24	3.35	2.0	0.29

[a] Adsorption time, 1day; temperature, 77 K.

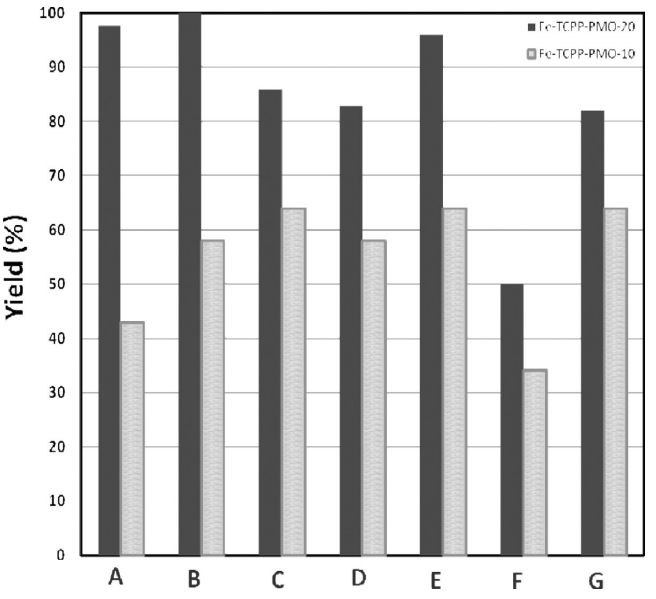

Figure 9. Baeyer–Villiger oxidation of various ketones using benzaldehyde under oxygen atmosphere ((A) Cyclopentanone; (B) Cyclohexanone; (C) Cycloheptanone; (D) Cyclooctanone; (E) Adamantanone; (F) 2-methylcyclohexanone; (G) 4-methylcyclohexanone).

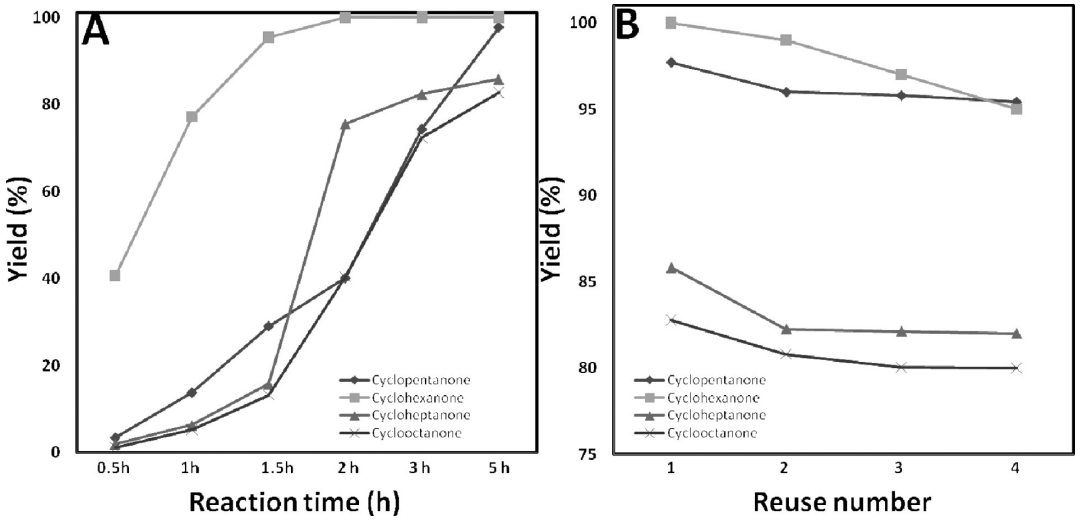

Figure 8. Effect of reaction time on Baeyer–Villiger oxidation of cyclohexanone by Fe-TCPP-PMO-20% (A) and cycle lifetime of Fe-TCPP-PMO-20% in the Baeyer–Villiger oxidation of cyclohexanone.

dx.doi.org/10.1021/cs200163r |ACS Catal. 2011, 1, 855–863

observed from the 2-methylcyclohexanone and 4-methylcyclohexanone. 50% 2-methylcyclohexanone and 82% 4-methylcyclohexanone were changed to the corresponding product under the same reaction conditions. (Figure 9 F,G)

4. CONCLUSION

In conclusion, we have developed an approach for the synthesis of the highly ordered periodic mesoporous organosilicas using from M-tetrakis(carboxyphenyl)porphyrin-silsesquioxanes as tetra-silanes by a thermal sol−gel method. The products showed the ordering and structure expected for an MCM-41 structure type. The M-TCPP-PMO-*n* (*n* = 10% and 20%) have highly textual properties such as surface area, pore diameter, total pore volume. The catalytic activity of M-TCPP-PMO-*n* catalyst was investigated in the liquid-phase Baeyer−Villiger oxidation of different cyclic ketones. There is a Fe-TCPP-PMO-20% to achieve the higher efficiency. Furthermore, the catalysts also had high durability which was demonstrated by a recyclability test.

■ ASSOCIATED CONTENT

Supporting Information. The pore size distributions of M-TCPP-PMO-10% and -20% (M = Fe, Cu, and Sn) calculated by the BJH method. This material is available free of charge via the Internet at http://pubs.acs.org.

■ AUTHOR INFORMATION

Corresponding Author

*Phone: +82 32 860-7675. Fax: +82 32 872 8670. E-mail: separk@inha.ac.kr.

Funding Sources

This work was supported by the Korea Science and Engineering Foundation (KOSEF) through the National Research Laboratory program funded by the ministry of science and technology (Project number: 2010-0018882).

■ REFERENCES

(1) Liu, Z.-B.; Zhu, Y.-Z.; Zhu, Y.; Chen, S.-Q.; Zheng, J.-Y.; Tian, J.-G. *J. Phys. Chem. B* **2006**, *110*, 15140–15145.
(2) Abrahams, B. F.; Hoskins, B. F.; Michail, D. M.; Robson, R. *Nature* **1994**, *369*, 727–729.
(3) Zhang, H.; Sun, Y.; Ye, K.; Zhang, P.; Wang, Y. *J. Mater. Chem.* **2005**, *15*, 3181–3186.
(4) Fungo, F.; Otero, L. A.; Sereno, L.; Silber, J. J.; Durantini, E. N. *Dyes Pigm.* **2001**, *50*, 163–170.
(5) Sakthitharan, S.; Edwards, C.; Boyle, R. *Tetrahedron* **2000**, *56*, 1025–1046.
(6) Jeong, E.-Y.; Ansari, M. B.; Mo, Y.-H.; Park, S.-E. *J. Hazard. Mater.* **2011**, *185*, 1311–1317.
(7) Que, L.; Tolman, W. B. *Nature* **2008**, *455*, 333–340.
(8) Ellis, P. E.; Lyons, J. E. *Coord. Chem. Rev.* **1990**, *105*, 181–193.
(9) Nam, W. *Acc. Chem. Res.* **2007**, *40*, 522–531.
(10) Zampronio, E.; Gotardo, M.; Assis, M.; Oliveira, H. *Catal. Lett.* **2005**, *104*, 53–56.
(11) Ebadi, A.; Safari, N.; Peyrovi, M. H. *Appl. Catal., A* **2007**, *321*, 135–139.
(12) Huang, G.; Liu, S.-Y.; Guo, Y.-A.; Wang, A.-P.; Luo, J.; Cai, C.-C. *Appl. Catal., A* **2009**, *358*, 173–179.
(13) Kameyama, H.; Narumi, F.; Hattori, T.; Kameyama, H. *J. Mol. Catal. A: Chem.* **2006**, *258*, 172–177.
(14) Halma, M.; Aparecida, K.; Freitas, D. D.; Taviot-gueho, C.; Prévot, V.; Forano, C.; Wypych, F.; Nakagaki, S. *J. Catal.* **2008**, *257*, 233–243.
(15) Tong, Z.; Shichi, T.; Zhang, G.; Takagi, K. *Res. Chem. Intermed.* **2003**, *29*, 335–341.
(16) Serwicka, E. M.; Poltowicz, J.; Bahranowski, K.; Olejniczak, Z.; Jones, W. *Appl. Catal., A* **2004**, *275*, 9–14.
(17) Asefa, T.; MacLachlan, M. J.; Coombs, N.; Ozin, G. A. *Nature* **1999**, *402*, 867–871.
(18) Asefa, T.; Kruk, M.; MacLachlan, M. J.; Coombs, N.; Grondey, H.; Jaroniec, M.; Ozin, G. A. *J. Am. Chem. Soc.* **2001**, *123*, 8520–8530.
(19) Burleigh, M. C.; Jayasundera, S.; Spector, M. S.; Thomas, C. W.; Markowitz, M. A.; Gaber, B. P. *Chem. Mater.* **2004**, *16*, 3–5.
(20) Hunks, W. J.; Ozin, G. A. *Chem. Mater.* **2004**, *16*, 5465–5472.
(21) Sayari, A.; Hamoudi, S. *Chem. Mater.* **2001**, *13*, 3151–3168.
(22) Singh, A.; Torita, N.; Shylesh, S.; Iwasa, N.; Arai, M. *Catal. Lett.* **2009**, *132*, 492–499.
(23) Yang, Q.; Li, Y.; Zhang, L.; Yang, J.; Liu, J.; Li, C. *J. Phys. Chem. B* **2004**, *108*, 7934–7937.
(24) Wan, Y.; Zhang, D.; Zhai, Y.; Feng, C.; Chen, J.; Li, H. *Chem.—Asian J.* **2007**, *2*, 875–881.
(25) Kapoor, M. P.; Yang, Q.; Inagaki, S. *J. Am. Chem. Soc.* **2002**, *124*, 15176–15177.
(26) Corriu, R. J. P.; Mehdi, A.; Reye, C.; Thieuleux, C. *Chem. Commun.* **2002**, 1382–1383.
(27) Grudzien, R. M.; Grabicka, B. E.; Pikus, S.; Jaroniec, M. *Chem. Mater.* **2006**, *18*, 1722–1725.
(28) Whitnall, W.; Cademartiri, L.; Ozin, G. A. *J. Am. Chem. Soc.* **2007**, *129*, 15644–15649.
(29) Jeong, E.-Y.; Burri, A.; Lee, S.-Y.; Park, S.-E. *J. Mater. Chem.* **2010**, *20*, 10869–10875.
(30) Harriman, A. *J. Chem. Soc., Faraday Trans.* **1981**, *77*, 369–377.
(31) Koerner, R.; Olmstead, M. M.; Ozarowski, A.; Phillips, S. L.; Calcar, P. M. V.; Winkler, K.; Balch, A. L. *J. Am. Chem. Soc.* **1998**, *120* (6), 1274–1284.
(32) Scalise, I.; Durantini, E. N. *J. Photochem. Photobiol. A.* **2004**, *162*, 105–113.
(33) Spasojević, I.; Colvin, O. M.; Warshany, K. R.; Batinić-Haberle, I. *J. Inorg. Biochem.* **2006**, *100*, 1897–1902.
(34) Khin, C.; Heinecke, J.; Ford, P. C. *J. Am. Chem. Soc.* **2008**, *130*, 13830–13831.
(35) Sharma, P. K.; Kevorkiants, R.; Visser, S. P. d.; Kumar, D.; Shaik, S. *Angew. Chem., Int. Ed.* **2004**, *116*, 1149–1152.
(36) Jinka, K. M.; Lee, S.-C.; Park, S.-E.; Jasra, R. V. *Stud. Surf. Sci. Catal.* **2008**, *174*, 1187–1190.
(37) Nekoksová, I.; Ilková, N.; Zukal, A.; Cejka, J. In *Studies in Surface Science and Catalysis*; Abdelhamid, S., Mietek, J., Eds.; Elsevier: New York, 2005; Vol. 156, pp 779−786.
(38) Murahashi, S.-I.; Oda, Y.; Naota, T. *Tetrahedron Lett.* **1992**, *33*, 7557–7560.
(39) Chen, C.-Y.; Li, H.-X.; Davis, M. E. *Microporous Materials* **1993**, *2*, 17–26.
(40) Fujii, H.; Yoshimura, T.; Kamada, H. *Inorg. Chem.* **1996**, *35*, 2373–2377.